PHYSICAL REVIEW B VOLUME 55, NUMBER 11 15 MARCH 1997-I

Nonparabolicity effects in the bipolar quantum-well resonant-tunneling transistor

K. P. Clark* and W. P. Kirk
Center for Nanostructure Materials and Quantum Device Fabrication, Engineering-Physics Building, Texas A&M University, College Station, Texas 77843-4242

A. C. Seabaugh
Corporate Research and Development, Texas Instruments Incorporated, Dallas, Texas 75265
(Received 16 September 1996)

A numerical calculation of quantum-well resonant electron-state energies in the bipolar quantum-well resonant-tunneling transistor (BiQuaRTT) is compared with experimental results. From the multiple-peak resonant-tunneling characteristics, the energies of resonant quasibound states of the BiQuaRTT's triangular quantum well are determined. The electron-state energies can be over 1 eV above the conduction-band edge, and are strongly influenced by conduction-band nonparabolicity, producing nearly equally spaced resonances in the BiQuaRTT. [S0163-1829(97)00511-0]

I. INTRODUCTION

The bipolar quantum-well resonant-tunneling transistor (BiQuaRTT) evolved from the resonant-tunneling diode, with a third terminal added to contact a heavily p-doped quantum well.[1] This allowed separate control of the potential in the quantum well, the base of the transistor, and negative differential transconductance characteristics. A later variation of the BiQuaRTT, which we will discuss here, uses quasithermalized minority carriers injected into the states of a nearly triangular quantum well.[2–4] This resulted in multiple negative differential (direct) conductance effects with current gain at room temperature. In this paper, we compare results of a numerical model of the BiQuaRTT resonances with experimental results from devices with different quantum-well widths. A simple model of effective mass nonparabolicity in the numerical model provides good agreement with experiment.

The band profile of a typical BiQuaRTT is shown in Fig. 1 (the BiQuaRTT transistor action has been detailed in Refs. 2 and 3). A quantum well is formed by the built-in electric field in the base-collector junction adjacent to the collector tunnel barrier, shown by the inset of Fig. 1. Quantum states of this nearly triangular base-collector quantum well produce multiple negative differential resistance effects. This is shown in the I-V characteristics of Figs. 2 and 3 for two different base-collector well widths. As the collector-base voltage V_{CB} increases, the quantum well becomes deeper and the electron states move to lower energies. Transmission resonances occur as each quasibound state aligns with the top of the well, at the energy of the conduction band in the quasineutral base. At low temperatures (4.2 K) (see Figs. 2 and 3) the incident thermalized electron energy distribution in the base is sharply peaked at low energies (<1 meV), allowing sharp resonances.

Nonparabolicity effects (energy-dependent effective mass) play a large role in the BiQuaRTT due to the high energies of the resonant states. Several methods have been used to treat nonparabolicity.[5,6] The energy effective mass $m_E^*(E)=m^*(1+\alpha E)$, containing a first-order correction term, is often used. Here, m^* is the electron effective mass at the conduction-band edge, E is the energy above the band edge, and α is the nonparabolicity parameter calculated from $\mathbf{k}\cdot\mathbf{p}$ theory. A two-band approximation yields $\alpha=(1-m^*/m_0)^2/E_G$, where m_0 is the free-electron mass and E_G is the band gap. For $\mathrm{In}_x\mathrm{Ga}_{1-x}\mathrm{As}$ ($m^*/m_0=0.041$, $E_G=0.812$ eV at 4.2 K), this yields $\alpha=1.13\ \mathrm{eV}^{-1}$. This value is close to the value $\alpha=1.3\ \mathrm{eV}^{-1}$ found from fitting quantum interference effects in experiments on $\mathrm{In}_x\mathrm{Ga}_{1-x}\mathrm{As}$ microstructures.[7] The highest BiQuaRTT resonances involve energies $E>1$ eV, where the energy effective mass more than doubles. Thus nonparabolicity effects can be expected to reduce the energies of the higher resonances strongly.

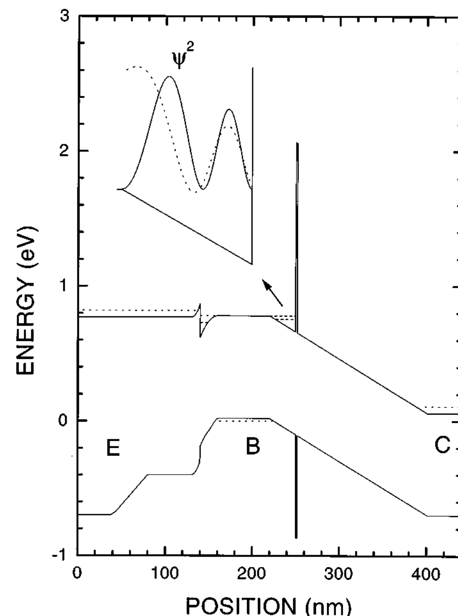

FIG. 1. Schematic energy-band profile of a BiQuaRTT with a base-emitter bias of 0.82 V and a collector-base bias of −0.11 V. An expanded view of the quantum well shows probability density corresponding to a quantum-well resonant state for both hard-wall (solid line) and soft-wall (dashed line) boundary conditions.

 © 1997 The American Physical Society

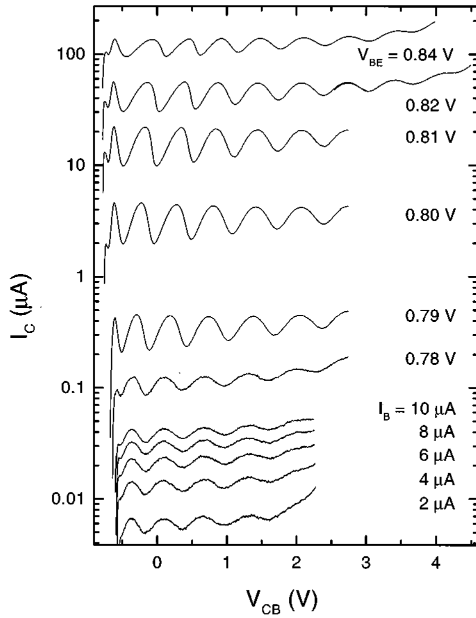

FIG. 2. BiQuaRTT current-voltage characteristics for a 30-nm well-width device at 4.2 K. The emitter-base junction is biased with a fixed applied voltage (curves in the upper part of figure) or with a fixed applied base current with emitter grounded (curves in the lower part of figure). Results are shown for 3R5660 HET4×4 4×4-μm^2 emitter size sample.

The BiQuaRTT structure allows the energy of the resonant states in relation to the band edge to be determined simply in a zero-temperature model, and space-charge effects can be avoided. The potential established in the p-type base is nearly independent of the electron current through the resonant states. Minority-carrier injection into resonant states has also been implemented in GaAs/Al_xGa_{1-x}As heterostructure bipolar transistors (HBTs) with resonant-tunneling double barriers in the collector.[8,9] In the BiQuaRTT, the base/collector quantum well is simply triangular to first order, formed by the applied base-collector electric field between a single heterobarrier and the edge of the base. Eigenstates and eigenenergies of this triangular well, including nonparabolicity, were obtained numerically. The numerical approach follows a method previously developed for quantum wells with an applied electric field.[10–12] Results for the experimental and simulated quantum-well eigenenergies are compared. We find nonparabolicity effects can account for the approximately equal spacing of the resonant peak voltages seen in the BiQuaRTT. Also of interest is the effect of the disorder potential in the base depletion layer adjoining the quantum well. This is probed in the calculation by two different quantum-state boundary conditions.

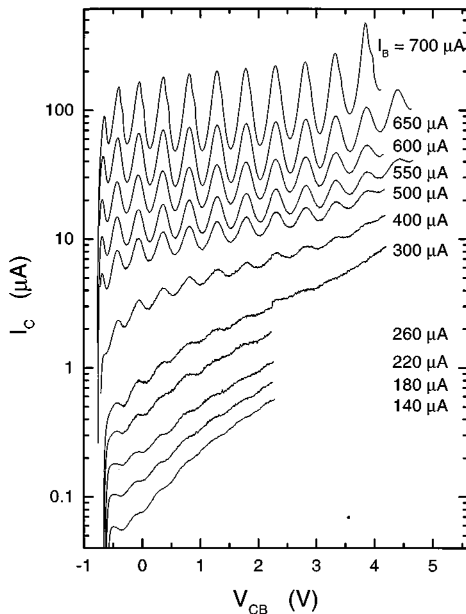

FIG. 3. BiQuaRTT current-voltage characteristics for 40-nm well device at 4.2 K, for several base-emitter voltage-bias conditions. Results are shown for 2R5429 CE4 4×20-μm^2 emitter size sample.

II. EXPERIMENT

The BiQuaRTT devices were fabricated at Texas Instruments with a triple-layer mesa process similar to conventional HBTs. The layer structure, yielding the data shown in Fig. 2, was grown by molecular-beam epitaxy on an InP substrate: a 1-μm In_xGa_{1-x}As collector contact layer (n 5 $\times 10^{18}$/cm^3), and 150-nm In_xGa_{1-x}As collector (undoped), 1.5-nm AlAs tunnel barrier, 30-nm In_xGa_{1-x}As quantum-well (undoped), 60-nm In_xGa_{1-x}As base (p 1×10^{19}/cm^3), 20-nm In_xGa_{1-x}As setback (undoped), 2-nm $In_{0.5}(Ga_{0.5}Al_{0.5})$As (undoped), 50-nm $In_{0.5}Ga_{0.5}Al_{0.5})_{0.5}$As emitter ($n$ 1×10^{18}/cm^3), 40-nm grading in composition and doping, 50-nm In_xAl_{1-x}As (n 5×10^{18}/cm^3), 40-nm compositional grading, and 320-nm In_xGa_{1-x}As contact (n 5×10^{18}/cm^3) layers. We also took data on other devices with 20- and 40-nm base-collector quantum-well regions. The 20-nm well-width layer structure differed slightly from the above, principally in 75-nm base thickness (p 5×10^{18}/cm^3), and 5-nm emitter-base setback layer. The 40-nm well-width samples had a 60-nm base thickness (p 5×10^{18}/cm^3), and a 2-nm AlAs barrier thickness. All the samples were bonded in ceramic dual in-line packages, and cooled to 4.2 K for the measurements.

From the I-V curves, we determine the voltage position of the current peaks $V_{CB,PK}$. The shift of the $V_{CB,PK}$ values slightly to the right in the higher current curves in Figs. 2 and 3 is reasonable since higher currents increase electron space charge in the well, changing the internal field, and increasing the resonant energies. The lowest V_{CB} peaks in Fig. 3 do not shift to higher V_{CB} as the resonant current increases. This may be due to hole space charge in the well at low V_{CB}, which compensates for the increase of the electron charge. However, the $V_{CB,PK}$ shift can be complicated by base resistance effects. In data from two 20-nm well-width devices, of emitter sizes 1×9 and 3×19 μm^2, $V_{CB,PK}$ shifted to lower voltages at higher currents. The lateral voltage drop in the base layer causes the measured $V_{CB,PK}$ to be lower than the intrinsic $V_{CB,PK}$, as reported for a HBT with a double-barrier resonant-tunneling collector.[9] In our devices, at low temperatures, lateral electron diffusion dominates the base current, complicating calculation of the voltage drop. To minimize this parasitic resistance effect, and to minimize effects of

space charge accumulation in the well, $V_{CB,PK}$ values were found from averaging low bias ($I_B<10$ μA, $I_C<1$ μA) results. However, the lowest V_{CB} peaks, and those for V_{CB} above about 3 V, required higher bias conditions to be observed. The peak voltages for the 30-nm well width (Fig. 2) were $V_{CB,PK}=-0.74$, -0.60, -0.36, 0.11, 0.67, 1.31, 1.95, 2.73, and 3.33 V. For the 40-nm well width (Fig. 3), $V_{CB,PK}=-0.68$, -0.50, -0.14, 0.27 0.72, 1.20, 1.68, 2.18, 2.78, 3.34, 3.86, and 4.37 V. For 20-nm devices the average $V_{CB,PK}=-0.36$, 0.44, 1.33, 2.31, and 3.18 V.

To find the quantum-well energy depth E_n for each $V_{CB,PK}$, we first calculate the slope a_n of the conduction band in the well as given by

$$a_n=e|\mathbf{E}|=(eV_{CB,PK}+E_G)/(L_C+L_B+L_W). \tag{1}$$

Here a_n is in units of eV/μm, $\mathbf{E}$ is the electric field in the well, L_C, L_B, and L_W are the thicknesses of the undoped collector, barrier, and well, and E_G is the effective band gap in the doped part of the base. A constant electric field throughout the undoped well, barrier, and collector is assumed, as the thermal diffusion of carriers into the undoped regions is suppressed at low temperatures. We employ an interesting technique for determining E_G by using magneto-oscillation measurements of the two-dimensional electron gas (2DEG) formed at the emitter-base interface.[13] This 2DEG is shown on the left-hand side of the base in Fig. 1. At low applied V_{BE}, the 2DEG Fermi level is in equilibrium with the emitter Fermi level, and the 2DEG density increases with V_{BE}. However, as V_{BE} increases to a point where the 2DEG Fermi level nearly aligns with the conduction-band edge in the base, emission into the base limits the 2DEG density. The crossover point is inferred from measurements of the 2DEG density at 4.2 K which show a density maximum at V_{BE}=780 mV; hence we estimate E_G=780 meV. Having obtained a_n, the base-collector quantum-well depth is then $E_n=a_nl$, where $l=(L_w+l_d/2)$ is the effective well width. The effective well width includes a small correction due to l_d, the simple depletion length of the base, where $a_nl_d/2$ is the potential energy drop across the depletion region.

III. NUMERICAL CALCULATION

An analytical estimate for the BiQuaRTT resonance energies is provided by the eigenenergies of an infinite triangular well. These are approximately

$$E_n=\left(\frac{\hbar^2}{2m^*}\right)^{1/3}\left(\frac{3\pi a_n}{2}\right)^{2/3}\left(n+\frac{3}{4}\right)^{2/3}, \tag{2}$$

where m^* is the effective mass (assumed parabolic). The resonance condition of the BiQuaRTT, $E_n=a_nl$, then yields the well depth at resonance,

$$E_n=\frac{\hbar^2}{2m^*l^2}\left[\frac{3\pi}{2}\left(n+\frac{3}{4}\right)\right]^2. \tag{3}$$

This implies that E_n, and therefore the $V_{CB,PK}$ values will vary as $\sim n^2$. However, from Figs. 2 and 3 we observe nearly equally spaced peaks. The discrepancy is attributed in large part to nonparabolic mass effects, which cause an increase in mass with energy, and reduces the energies of the higher resonance levels.

To account for the nonparabolic mass, numerical techniques can be used. The electron envelope function in the well satisfies

$$\frac{\hbar^2}{2}\frac{\partial}{\partial z}\left(\frac{1}{m^*(E)}\frac{\partial\Psi}{\partial z}\right)+V(z)\Psi=E\Psi, \tag{4}$$

where the mass $m^*(E)=m^*(1+\alpha E)$ implicitly depends on z through E. For a numerical solution, the equation is converted into three coupled linear first-order equations by the substitution $y_1=\Psi$, $y_2=(1/m^*(E))\partial\Psi/\partial z$, and $y_3=E$.[10–12] Using the relaxation method, the first-order equations for the y_i are discretized on a 1D uniform grid inside the interval $z=0$ (barrier side of well) to $z=L_w+l_d$ (doped base side of well).[12] The transmission resonance occurs when a state is at the top of the triangular quantum well, aligned with the energy of the incident thermalized electrons. In general, for this virtual resonance, ''open'' boundary conditions are needed.[14] However, the incident energies are only slightly above ($k_BT<\sim0.4$ meV) the top of the well, and we approximate the resonance as a purely bound state with an energy just below (0.1 meV) the top of the well. Outside the well, on each side the potential is taken as constant as in the Bardeen transfer Hamiltonian approach. This allows an analytical expression for the (exponentially decaying) wave function outside of the well. In the barrier, a direct-gap conduction-band offset of 1.27 eV and the nonparabolic energy effective mass is used. The wave-function boundary conditions at $z=0$ and $z=l_w+l_d$ rely on the continuity of the wave function (y_1) and the first derivative divided by the effective mass (y_2). We obtain a boundary condition relating the wave function at the barrier $y_1(z=0)$ to the derivative $y_2(z=0)$. On the base side, the matching conditions were imposed with the eigenenergy 0.1 meV below the conduction-band edge in the base, yielding a boundary condition relating $y_1(z=L_w+l_d)$ and $y_2(z=L_w+l_d)$. Given an initial value for a_n, the initial guess for the wave function was provided by an Airy function. After solving for y_i, the boundary conditions were adjusted to relax to the correct values, and the solution was repeated. This entailed changing $y_1(z=0)$, $y_1(z=L_w+l_d)$, l_d, and a self-consistently, so the boundary conditions were satisfied with the eigenenergy aligned with the top of the well.

The exact potential at the interface between the quantum well and the doped part of the base is not well known, and we used two opposite resonant state boundary conditions. In the basic model discussed above, the conduction band in the doped base is assumed to be constant, and the resonant state energy is only slightly below this potential, which yields a long wave-function decay length into the doped base. This ''soft-wall'' boundary condition corresponds to the dotted curve in the inset of Fig. 1. However, this model may break down due to the high density of ionized impurities, and potential fluctuations, in the depletion region at the edge of the doped base. Each negatively charged ionized acceptor in the base depletion region produces a very large repulsive potential at short range, and presumably a node in the quantum-well wave function. The envelope-function wavelength in

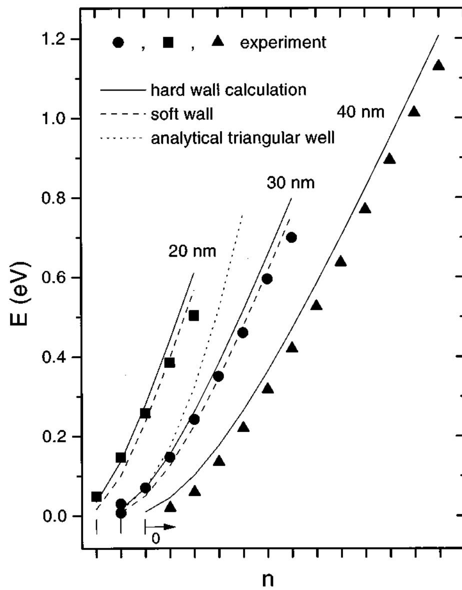

FIG. 4. Quantum-well energy E_n vs resonance number n for devices with 20-, 30-, and 40-nm base-collector well thicknesses. Experimentally derived data: solid points. Calculated results: analytical (dotted line), numerical with soft-wall (dashed lines), and hard-wall (solid lines) boundary conditions. Lines connecting the calculated points are to guide the eye.

the plane of the quantum well ($h/\sqrt{2m^*k_BT}\approx 300$ nm at 4.2 K) exceeds the separation of the ionized impurities (approximately 10–60 nm for base-collector electric fields 0.4–25 V/μm). The nodes at ions may result in an overall minimum of the wave function in the depletion layer. This was included as an alternate boundary condition of a wave-function node in the depletion layer at $z=L_w+l_d$. This ''hard-wall'' boundary condition corresponds to the solid curve in the inset of Fig. 1.

IV. RESULTS AND DISCUSSION

The experimentally and numerically derived resonant state energies E_n are shown in Fig. 4. The experimental values are shown as the solid points, while the theoretical values are connected by a line to guide the eye. The dotted line shows the analytical model results for the 30-nm well, without corrections for nonparabolicity or base depletion. The dashed lines are the numerical model results using the soft-wall boundary condition, while the solid lines embody the result of using the hard-wall boundary condition.

The 30-nm experimental data had two peaks at the lowest energies (7 and 30 meV), while the theoretical models predicted only one (~18 meV). We have plotted both experimental low-energy peaks at $n=0$ to allow a better fit for peaks at $n=1$–3. At present, it is not clear what causes the presumed extra experimental peak at low energy. At low V_{CB}, the base-collector junction is nearly flatband, and the constant electric-field model breaks down due to residual impurities and carrier diffusion into the collector. Hole charge diffusing into the well region contributes an attractive potential, which could lower the experimental $n=0$ peak energy.[15] Also, the lowest observed peak is partially cut off at low V_{CB} by the transistor turn-on characteristics, so the actual peak voltage could not be obtained.

The 40-nm experimental E_n vs n results, plotted starting at $n=1$, have a slope similar to that of the calculated results, but were all about 40 meV lower in energy. One possibility that could account for this is residual doping in the collector or barrier. For example, ionized donors of n $1.4\times 10^{16}/\mathrm{cm}^3$ in the collector would produce a built-in field sufficient to shift all the resonance energies by 40 meV.

The analytical model (dotted curve shown for the 30-nm data) produced resonance energies in good agreement at low energies, but diverge from the nearly linear experimental E_n vs n results at high energies. Over a large energy range above 200 meV, the experimental resonance energies are nearly equally spaced. The linear E_n vs n dependence is seen also in the numerical models which include nonparabolicity. For energies above 200 meV, the experimental energies are lower than the numerical results. The first-order nonparabolic mass model cannot be expected to be accurate at these energies. However, no very large deviation is seen from the experimental data over the entire range of energy.

For both 20- and 30-nm well widths, the hard-wall boundary condition (solid line) produces somewhat better agreement with the data than the soft-wall boundary condition (dashed line) at low energies. This supports the picture that ionized acceptors in the base depletion layer form the edge of the quantum well. This is important for transport, since the mean free path cannot exceed the wave-function penetration of a potential barrier.[16] However, the current results are not conclusive since the different boundary value assumptions tend to shift all the energies by nearly the same amount, similar to experimental parasitics such as residual doping in the collector.

V. CONCLUSION

The quantum-well resonance energies for 20-, 30-, and 40-nm width base-collector well BiQuaRTT's were obtained from the corresponding measured resonant peak voltages. A simple numerical model treating the resonant states in a bound-state approximation produces results that fit the experimental results well. The principal conclusion is that the nonparabolic effective mass results in a nearly equal spacing of BiQuaRTT resonance voltages corresponding to quantum-well energies above 200 meV. Data from 20- and 30-nm devices also support a hard-wall model for the effect of the base depletion layer on the wave function. Further work is needed on the lowest-voltage peak and the influence of residual doping.

ACKNOWLEDGMENTS

We gratefully acknowledge discussions with W. R. Frensley, R. E. Allen, and T. C. Zhou. This work was supported in part by the Texas Advanced Research Program under Grant No. 999903-213.

*Electronic address: kevin@nanofab.tamu.edu

[1] M. A. Reed, W. R. Frensley, R. J. Matyi, J. N. Randall, and A. C. Seabaugh, Appl. Phys. Lett. **54**, 1034 (1989).
[2] A. C. Seabaugh, Y. C. Kao, W. R. Frensley, J. N. Randall, and M. A. Reed, Appl. Phys. Lett. **59**, 3413 (1991).
[3] A. C. Seabaugh and M. A. Reed, in *Heterostructures and Quantum Devices*, edited by N. G. Einspruch and W. R. Frensley (Academic, New York, 1994), pp. 351–383.
[4] A. C. Seabaugh, E. A. Beam, Y. C. Kao, J. H. Luscombe, and J. N. Randall, OSA Proc. Ultrafast Electron. Optoelectron. **14**, 65 (1993).
[5] U. Ekenberg, Phys. Rev. B **40**, 7714 (1989).
[6] M. Heiblum and M. V. Fischetti, in *Physics of Quantum Electron Devices*, edited by F. Capasso (Springer, Berlin, 1989), pp. 274–275.
[7] L. Eaves, F. W. Sheard, and G. A. Toombs, in *Physics of Quantum Electron Devices*, edited by F. Capasso (Springer, Berlin, 1989), p. 127 and references therein.
[8] K. Berthold, A. F. J. Levi, J. Walker, and R. J. Malik, Appl. Phys. Lett. **54**, 813 (1989).
[9] N. Shigekawa, P. H. Beton, H. Buhmann, L. Eaves, M. Henini, and D. Johnston, Semicond. Sci. Technol. **9**, 1500 (1994).
[10] W. Chen and T. G. Andersson, Phys. Rev. B **44**, 9068 (1991).
[11] W. L. Bloss, J. Appl. Phys. **65**, 4789 (1989).
[12] W. H. Press, B. P. Flannery, S. A. Teukolsky, and W. T. Vettering, *Numerical Recipes in C. The Art of Scientific Computing* (Cambridge University Press, Cambridge, 1987), p. 617.
[13] K. P. Clark, W. P. Kirk, A. C. Seabaugh, and Y.-C. Kao, J. Appl. Phys. **79**, 2732 (1996).
[14] W. R. Frensley, Superlatt. Microstruct. **11**, 347 (1992).
[15] O. V. Konstantinov and O. A. Mezrin, Fiz. Tekh. Polopruvodn. **18**, 2166 (1984) [Sov. Phys. Semicond. **18**, 1355 (1984)].
[16] I. M. Lifshitz and V. Ya. Kirpichenkov, Zh. Eksp. Teor. Fiz. **77**, 989 (1979) [Sov. Phys. JETP **50**, 502 (1979)].